In Vitro Cell.Dev.Biol.—Animal (2017) 53:632–645
DOI 10.1007/s11626-017-0150-5

Interaction of silver and gold nanoparticles in mammalian cancer: as real topical bullet for wound healing— A comparative study

Allur Subramaniyan Sivakumar[1] · Chandran Krishnaraj[2] · Sunirmal Sheet[3] · Dileep Reddy Rampa[4] · Da Rae Kang[1] · Shah Ahmed Belal[1] · Abhay Kumar[5] · In Ho Hwang[6] · Soon-Il Yun[2] · Yang Soo Lee[3] · Kwan Seob Shim[1]

Received: 16 January 2017 / Accepted: 24 March 2017 / Published online: 1 May 2017 / Editor: Tetsuji Okamoto

Abstract The present study evaluates in vitro cytotoxic effects and the mode of interaction of biologically synthesized Ag and Au nanoparticles (NPs) using *Brassica oleracea* L. var. *capitata* f. *rubra* (*BOL*) against HT-1080 cancer cells and bacterial cells as well as their wound healing efficacy using a mouse model. UV–visible spectroscopy, scanning electron microscopy, high-resolution transmission electron microscopy, and energy-dispersive X-ray analysis have ascertained the formation of nano-sized Ag and Au particles. Fourier transform infrared analysis has confirmed that polyphenol and amide groups in *BOL* act as capping as well as reducing agents. The free radical scavenging activity under in vitro conditions is found to be higher for the Ag NPs when compared to the Au NPs. Acridine orange–ethidium bromide dual staining and comet assay have indicated that the cytotoxic effects are mediated through nuclear morphological changes and DNA damage. The intracellular localization of Ag and Au NPs in HT-1080 cells and their subsequent effect on apoptosis and necrosis were analyzed by flow cytometry while the mode of interaction was established by scanning electron microscopy under field emission mode and by bio-transmission electron microscopy. These methods of analysis clearly revealed that the Ag and Au NPs have easily entered and accumulated into the cytosol and nucleus, resulting in activation of inflammatory and apoptosis pathways, which in turn cause damage in DNA. Further, mRNA and protein expression of caspase-3 and caspase-7, TNF-α, and NF-κB have provided sufficient clues for induction of intrinsic and extrinsic apoptosis and inflammatory pathways in Ag NP- and Au NP-treated cells. Evaluation of wound healing properties of Ag and Au NPs using a mouse model indicates rapid healing of wounds. In addition, no clear toxic effects and no nuclear abnormalities in peripheral blood cells are observed. Ag NPs appear to be a better anticancer therapeutic agent than Au NPs. Nonetheless, both Ag NPs and Au NPs show potential for promoting topical wound healing without any toxic effects.

Keywords Silver · Gold · Nanoparticles · Apoptosis · Cancer · Wound healing · Inflammation · Peripheral blood

Electronic supplementary material The online version of this article (doi:10.1007/s11626-017-0150-5) contains supplementary material, which is available to authorized users.

✉ Kwan Seob Shim
ksshim@jbnu.ac.kr

[1] Department of Animal Biotechnology, Chonbuk National University, Jeonju 561-756, Republic of Korea

[2] Department of Food Science and Technology, Chonbuk National University, Jeonju 561-756, Republic of Korea

[3] Department of Wood Science and Technology, College of Agriculture and Life Sciences, Chonbuk National University, Jeonju 561-756, Republic of Korea

[4] Department of BIN Convergence Technology, College of Engineering, Chonbuk National University, Jeonju 561-756, Republic of Korea

[5] R&D Centre, M/s. Eureka Forbes Limited, Kudlu, Bangalore, India

[6] Department of Animal Science, Chonbuk National University, Jeonju 561-756, Republic of Korea

Introduction

Currently, cancer is a major issue in human health, and it is the second leading cause of death in economically developed countries. It is characterized by abnormal cell growth and is a multistep process caused by changes in the genetic background, influenced by environmental factors (Lafon-Hughes et al. 2008). Many types of cancer therapies are currently being practiced, and considerable advancements are

constantly being researched. Recently, nanotechnology has emerged as a potential solution for many problems, and it is considered to create a paradigm change in the detection, treatment, and prevention of cancer (NCI report) (Pardee and Stein 2011). Nanoparticles (1–100 nm in size) can be engineered to offer multifunctional capabilities: to act as an imaging agent that could detect, target, and deliver a therapeutic drug in cancer therapy and also to increase drug efficacy with low toxicity (Nasongkla et al. 2006).

Numerous methods are hitherto available for the synthesis of nanoparticles (NPs), which include physical, chemical, and biological methods and hybrids. The chemical and physical methods of the synthesis of NPs require the addition of toxic chemicals, some of which may be very expensive. In addition, these methods involve a complex reaction sequence. In contrast, the biological method is considered to be environment friendly, nontoxic, and cost-effective for the synthesis of NPs. Several researchers have explored the possibility of synthesizing NPs using diverse biological methods using plant extracts and microorganisms like bacteria, yeasts, fungi, and algae (Salunke et al. 2014). All of these methods are promising and deliver multiple therapeutic agents to cancer cells. Plant-mediated syntheses of metal NPs including silver, gold, palladium, iron, copper, zinc, and titanium have been reported. Among them, Ag NPs have shown promise as a therapeutic agent, particularly in cancer therapy, food safety, and water purification (Kumar and Mamidyala 2011). It is interesting to note that plant-mediated synthesis of Ag NPs has induced cytotoxicity and genotoxicity in many cancer cells such as Hep-G2 (hepatic cancer), MCF-7 (breast cancer), HCT-15 (colon cancer), HeLa, and THP-1. The use of Ag NPs has caused apoptosis, altered cell morphology, reduced cell viability, and generated oxidative stress, leading to lipid peroxidation of biological membranes and damage of structural proteins and DNA (Foldbjerg et al. 2009). Ag NPs have been used for tomography imaging (Liu et al. 2013), as a biosensor (Singh et al. 2013), for environmental sensing (Saha et al. 2012), for water purification (Pradeep 2009), for DNA labeling, and for vapor sensing applications.

Brassica oleracea L. var. *capitata* f. *rubra* (*BOL*) (red cabbage) possesses the highest free radical scavenging, antioxidant, antifungal, antibacterial, and anticancer properties (Singh et al. 2006). The red cabbage extract has reduced the proliferation of human colon cancer cells and increased the pro-apoptotic activity. The main ingredients of the *BOL* extract are alkaloids, phenolic compounds, carotenoids, vitamin C, quercetin, kaempferol, and anthocyanins (Ahmed and Rao 2014). These compounds are known to act as reducing as well as stabilizing agents in the bio-reduction of silver and gold. Synthesis of metal NPs using the *BOL* extract has not been explored previously. In this perspective, the present study aims to synthesize Ag and Au NPs using an aqueous extract of *BOL*. The study also aims to demonstrate the cytotoxic effects including the apoptotic effect of Ag and Au NPs on human-derived fibrosarcoma cells (HT-1080), the interplay of pro-apoptotic caspase-3 and caspase-7 in the apoptotic process by quantitative real-time polymerase chain reaction (qRT-PCR), and the internal localization of different concentrations of Ag and Au NPs in the cytoplasm and nucleus of HT-1080 cells.

Materials and Methods

Materials Fresh and healthy leaves of *B. oleracea* L. var. *capitata* f. *rubra* (*BOL*) (red cabbage) were procured from the local market in Jeonju, South Korea. Silver nitrate ($AgNO_3$) and gold chloride ($HAuCl_4$) were purchased from Sigma-Aldrich Chemicals Co. (254169; St. Louis, MO). The mouse myoblast human-derived fibrosarcoma cells (HT-1080) were purchased from the American Type Culture Collection (ATCCCRL 1772; Manassas, VA). The iScript™ cDNA Synthesis Kit (170-8891) and SsoFast EvaGreen Supermix (172-5202) were procured from BIO-RAD Laboratories, Inc. (Hercules, CA). Primers were obtained from Genotech (Daejeon, South Korea). Dulbecco's modified Eagle's medium (DMEM) was purchased from Life Technologies (Grand Island, NY). Cell Growth Determination Kit, 1,1-diphenyl-2-picrylhydrazyl (DPPH), 2,2′-azino-bis(3-ethylbenzthiazoline-6-sulfonic acid) (ABTS), acridine orange (AO), and ethidium bromide were purchased from Sigma-Aldrich Chemicals Co.

Synthesis of Ag and Au NPs Ten grams of fresh and healthy leaves of *BOL* were cleaned with tap water, followed by deionized water several times to remove any external particles adhered on their surface, and boiled in 100 ml of deionized water for 5 min in a microwave oven, and the resulting extract was filtered through a Whatman filter paper. Two different sets of reaction mixture (6 ml of extract + 44 ml of $D.H_2O$) were prepared. To them, 1 mM $AgNO_3$ and 1 mM $HAuCl_4$ were added, and they were kept in the dark at room temperature. A control setup was also maintained throughout the experiment with the leaf extract alone.

Characterization of Ag and Au NPs An aliquot of the reaction mixture was sampled at regular intervals and analyzed using UV–visible spectroscopy (UV-1800, Shimadzu, Kyoto, Japan) in the wavelength range of 200 to 800 nm. Further, the reaction mixture was centrifuged at 15,000 rpm for 20 min, and it was collected in the form of pellets. A portion of pellets was dispersed in 0.1 ml of ultrapure water and used for further characterization. For electron microscopy studies, 25 μl of the reaction mixture was coated on a copper grid and the images of Ag and Au NPs were observed using high-resolution transmission electron microscopy (HR-TEM)

(JEM-2010) while those coated using osmium were observed using scanning electron microscopy with a field emission mode (FE-SEM) (S-4800, Hitachi, Tokyo, Japan). Energy-dispersive X-ray analysis (EDS) and X-ray diffraction (XRD) measurement (X'Pert MRD, Philips, Netherlands) were used to determine the composition and phase content. A portion of the reaction mixture was freeze-dried with a concentrator from ilShinBioBase (Model No.: MCF D8512; Dongducheon, South Korea), and the resulting powder was used for analysis of functional groups by Fourier transform infrared (FT-IR) spectroscopy.

Antiradical activity of Ag and Au NPs. DPPH· and $ABTS^{+}$ The DPPH· radical scavenging activity was determined spectrophotometrically by the method of Brand-Williams et al. (1995). The reagents were added in the following order: 1 ml of DPPH· followed by varying concentrations of Ag NPs (100, 200, 300, 400, and 500 μM) and Au NPs (100, 200, 300, 400, and 500 μM) prepared using methanol. To this, 1 ml of DPPH· solution (0.2 mM/ml methanol) was added, and the contents were mixed well. The mixture was kept in the dark at 20°C for 40 min. After incubation, absorbance was measured at 517 nm using a UV–visible spectrophotometer with methanol as the blank. In this method, ascorbic acid was used as the standard.

The $ABTS^{\cdot+}$ radical inhibition activity of peptides was measured by the method of Woolfenden and Wilson (1982). $ABTS^{\cdot+}$ was dissolved in water at a concentration of 7 mM. The stock solution was mixed with 2.45 mM potassium persulfate (final concentration). The mixture was reacted for 12 h in the dark and then diluted using ethanol to obtain an absorbance of 0.7 at 734 nm. Different concentrations of Ag NPs (100, 200, 300, 400, and 500 μM) and Au NPs (100, 200, 300, 400, and 500 μM) were mixed with the ABTS solution (2980 μl), and the absorbance of the mixture at 734 nm was monitored after 15 min.

In vitro anticancer studies of Ag and Au NPs using cell culture. Cell culture and maintenance The HT-1080 cells were grown in 75-cm^2 flasks incubated at a density of 7000 cells/cm^2 and grown in DMEM supplemented with 10% FBS and penicillin (100 U/ml) in humidified atmosphere with 5% CO_2 at 37°C, and the medium was changed every 3 d. After reaching 80–90% confluence, the cells were harvested from the subconfluent monolayer after their detachment by exposure to trypsin containing 5.3 mM EDTA at 37°C for 5 min. Exposure to different concentrations of Ag and Au NPs was carried out on subconfluent cells. Cell confluence was assessed using inverted microscopy visualization (NXE0228, LOMO, St. Petersburg, Russia).

Experimental groups and exposure conditions In order to evaluate the effects of apoptotic pathways, HT-1080 cells were treated with different concentrations of Ag NPs (5, 10, 20, 40, 60, and 100 μg) and Au NPs (5, 10, 20, 40, 60, and 100 μg) separately for 24 h. The details of the experimental protocol are given in Table 1.

Evaluation of cytotoxicity by MTT assay Cultured HT-1080 cells at a concentration of 1×10^5 cells/ml were taken in a 96-well plate. Subsequently, the cells were pretreated with different concentrations of Ag or Au NPs (5, 10, 20, 40, 60, 80, and 100 μg/ml) for 24 h. MTT solution, in an amount equal to 10% of the culture volume, was added under sterile conditions and incubated for 3 to 4 h. Subsequently, the cultures were removed from the incubator, and the resulting MTT formazan was dissolved. Then, MTT solvent, in an amount equal to the original culture volume, was directly added to the culture, and the plates were read within 1 h at 570 nm using an ELISA-type plate reader equipped with appropriate filters.

AO/EtBr dual staining to detect apoptosis AO and ethidium bromide (EtBr) staining was used to detect the dead cells by nuclear staining (Lakshmi et al. 2008). The stained cells were viewed under the fluorescence microscope LSM 510 META (Carl Zeiss, Jena, Germany). The apoptotic cells were counted as a function of the total number of cells present in the field.

Single-cell gel electrophoresis (comet assay) DNA damage was estimated by alkaline single-cell gel electrophoresis (comet assay) according to the method of Singh et al. (1988). Briefly, with little modification, a layer of 1% NMPA was prepared on microscope slides. After NP treatment, HT-1080 cells were mixed with 200 μl of 0.5% LMPA. The slides were immersed in cold lysis solution at pH 10 (2.5 M NaCl, 10 mM Na_2EDTA, 10 mM Tris pH 10, 1% Triton X-100, 10% DMSO) and kept at 4°C for 60 min. To allow denaturation of DNA, the slides were placed in alkaline electrophoresis buffer at pH 13 and left for 25 min. The slides were neutralized in 0.4 M Tris (pH 7.5) for 5 min and stained with 20 mg/ml of EtBr. For visualization of DNA damage,

Table 1. Experimental groups

Serial no.	Treatment
Group 1	Control cells
Group 2	Control + Ag NPs/Au NPs (5 μg/ml)
Group 3	Control + Ag NPs/Au NPs (10 μg/ml)
Group 4	Control + Ag NPs/Au NPs (20 μg/ml)
Group 5	Control + Ag NPs/Au NPs (40 μg/ml)
Group 6	Control + Ag NPs/Au NPs (60 μg/ml)
Group 7	Control + Ag NPs/Au NPs (80 μg/ml)
Group 8	Control + Ag NPs/Au NPs (100 μg/ml)

At the end of the incubation period, the cells were used for further studies

observations were made using a 409 objective in an epifluorescent microscope equipped with an excitation filter of 510–560 nm and a barrier filter of 590 nm. DNA damage was quantified by tail moment, tail length, and olive tail moment (OTM). OTM is the product of the distance (in the *x* direction) between the center gravity of the head and the center gravity of the tail and the percent tail DNA.

Determination of apoptosis and necrosis FITC/PI Annexin V Apoptosis Detection Kit (BioLegend, Cat # 640914, San Diego, California, United States) was used to detect the apoptosis and necrosis rates of Ag NP- and Au NP-treated HT-1080 cells according to the manufacturer's instructions. After incubation with Ag NPs and Au NPs for 48 h, HT-1080 cells were harvested, washed with PBS, suspended in Annexin V binding buffer, and incubated with FITC-labeled Annexin V and PI for 15 min at room temperature in the dark. Then, the samples were immediately analyzed by flow cytometry (BD, Franklin Lakes, NJ).

Anti-apoptotic and anti-inflammatory protein by qRT-PCR After treatment, total cellular RNA was extracted with RNeasy™ Mini Kit (Cat# 74104 and 74106) in accordance with the manufacturer's instructions from QIAGEN (Hilden, Germany). Complementary DNA (cDNA) was synthesized using 2 μg of total RNA by iScript™ cDNA Synthesis Kit from BIO-RAD. Reverse transcription polymerase chain reaction (RT-PCR) assays were performed using CFX96™ Real-Time PCR Detection System (BIO-RAD). cDNA was amplified with each gene such as caspase-3 (cas-3) and caspase-7 (cas-7). The reaction was carried out according to the manufacturer's instructions. Statistical analysis of the real-time PCR results was performed by using the ΔCt value (Ct gene of interest − Ct reporter gene). Relative gene expression was calculated by the ΔΔCt method (ΔCt sample − ΔCt calibrator), with the use of the sham-operated group as a calibrator for comparison of all unknown sample gene expression levels. The conversion between ΔΔCt and relative gene expression levels is as follows: fold induction = $2^{-\Delta\Delta Ct}$, where $2^{-\Delta\Delta Ct}$ is the relative gene expression (Livak and Schmittgen 2001).

Anti-apoptotic and anti-inflammatory protein by western blot The cultured HT-1080 cells were exposed to increasing IC_{50} concentration of Ag NPs (40 μg/ml) and Au NPs (100 μg/ml) for 48 h, and the whole cell protein was isolated by using RIPA buffer for checking the protein expression of caspase-3, caspase-7, and TNF-α. Further, the nuclear protein was isolated for analyzing the NF-κB translocation as shown in our previous work (Sivakumar and Anuradha 2011). Protein concentration was determined using Bio-Rad Protein Assay Kit (BIO-RAD). A sample containing 25 μg of protein was solubilized in Laemmli buffer and separated by 6% acrylamide with 4% acrylamide stacking gel and then transferred into Hybond-P PVDF membranes (GE Healthcare, Amersham, UK) for 60 min at 200 mA. Then, the PVDF membranes were blocked using 5% skimmed milk powder in 0.5 M Tris-buffered saline, pH 7.4, with 0.05% Tween 20 (TBST) at room temperature for 2 h. Immunoblots were probed with caspase-3, caspase-7, TNF-α, and NF-κB primary antibody (1:5000 dilution) overnight. After three times of washing with TBST, the membranes were probed with HRP-conjugated secondary antibody (1:2000 dilution) for 60 min at room temperature. The membranes were then washed thrice with TBST for 10 min each. Protein bands were visualized using an enhanced chemiluminescence assay kit (WesternBright™ ECL, Advansta, Menlo Park, CA), scanned, and quantified using ImageJ software. The relative density ratio of the bands was normalized to GAPDH.

Mode of interaction of Ag and Au NPs with HT-1080 cell membranes For scanning electron microscopy (SEM), the cells were grown on coverslips in a six-well plate. After the experimental condition, the cells were fixed with 2% paraformaldehyde and 2% (vol/vol) glutaraldehyde at room temperature, then washed with washing solution (0.05 M sodium cacodylate buffer (pH 7.2)) and postfixed with 1% (vol/vol) osmium tetroxide in 0.05 M sodium cacodylate buffer (pH 7.2). Then, the coverslips were washed with washing solution followed by en block staining (1% (vol/vol) uranyl acetate). Dehydration was performed in a graded series of alcohol afterwards; the coverslips were air-dried at room temperature. Then, the coverslips were mounted on aluminum sample stubs and gold-coated by sputtering. Finally, the coverslips were observed by FE-SEM.

In vivo toxicity and wound healing. Animal and treatment Male ICR mice (20 g) were supplied by the Charles River Orient Experimental Animal Breeding Center (Seoul, South Korea). All animals were housed in wire cages at 20–22°C, with a relative humidity of 50 ± 10%, a frequency of air ventilation of 15–20 times/h, and 12-h illumination (07:00–19:00; intensity, 150–300 lx); fed standard laboratory chow (Charles River Orient Experimental Animal Breeding Center); and allowed water ad libitum. All procedures relating to the animals and their care conformed to the international guideline "Principles of Laboratory Animals Care" (NIH Publication No. 85-23, revised 1985). On the day of wounding, each mouse was anesthetized with ketamine (40 mg/kg) and xylazine (20 mg/kg) through the intraperitoneal route. Afterwards, dorsal hair was shaved and the skin was disinfected with iodine, and then a partial-thickness wound with a length of 8 mm was created. After that, the prepared wounds of the animals were divided into three groups containing six animals each: group 1, applied with Natrosol gel on the wound surface (control group); group 2, applied with Natrosol gel + 2.5 mg of Ag NPs; and group 3, applied with Natrosol gel + 2.5 mg of Au NPs. Each group of mice was housed separately. At the end of the experiment date (7th day), the

animals were sacrificed and blood was collected from heart. Immediately following blood collection, wound contraction was examined using the Image Analysis tool. Photographs were taken each day until the wounds perfectly healed.

Biochemical analysis To analyze the in vivo toxicity of formulation, biochemistry parameters (aspartate aminotransferase (AST) and alanine aminotransferase (ALT)) in blood plasma were studied using commercial kits.

Micronuclei and nuclear abnormality tests using periodic acid–Schiff staining Blood samples from the three groups were immediately smeared on clean grease-free microscope slides, allowed to air-dry, and fixed using methanol for 5 min, and the slides were gently rinsed with running tap water for 1 min, followed by immersion in periodic acid solution for 5 min at room temperature. Then, the slides were rinsed with $D.H_2O$, immersed in Schiff's reagent for 15 min at room temperature, and gently washed with running tap water for 5 min. Finally, they were counterstained with hematoxylin solution for 90 s, rinsed with running tap water for 30 s, allowed to air-

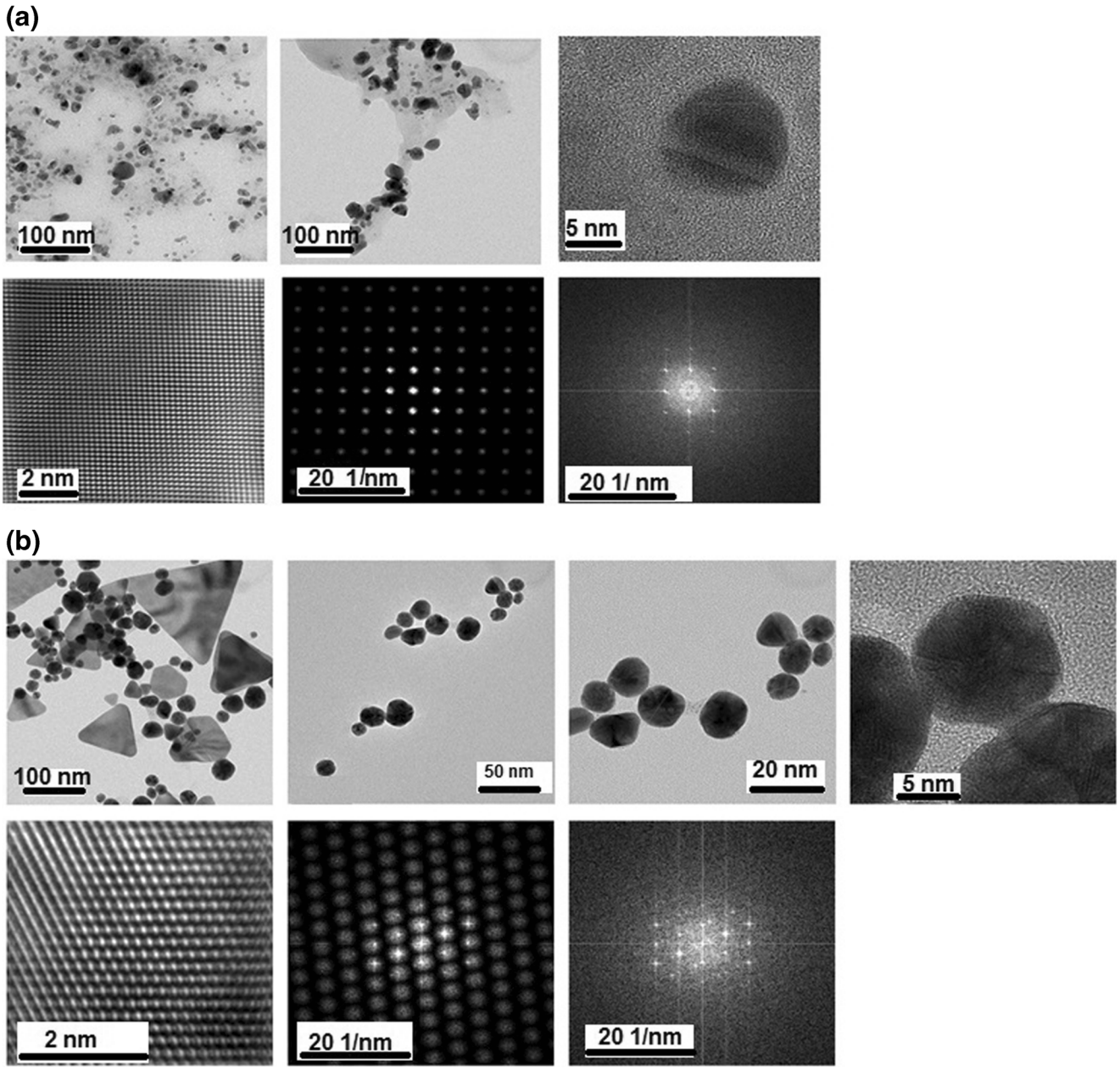

Fig. 1. HR-TEM analysis of polydispersed Ag and Au NPs observed with the addition of 1 mM $AgNO_3$ and 1 mM $HAuCl_4$ into aqueous *Brassica oleracea* L. var. *capitata* f. *rubra* extract. (*a*) Ag NPs. (*b*) Au NPs.

dry, and examined under a light microscope using mineral oil (×100).

Statistical analysis Data for biochemical analysis are mean ± SD (n = 6). Statistical evaluation was carried out by one-way analysis of variance (ANOVA), followed by Duncan's multiple range test (DMRT). A value of $p < 0.05$ was considered statistically significant.

Results and Discussion

Characteristics of Ag and Au NPs The aqueous *BOL* extract is pale pink in color. Addition of $AgNO_3$ and $HAuCl_4$ has changed the color of the solution to reddish brown and pinkish violet, respectively, within 2 h. UV–visible spectra of the solution exhibit absorption maxima at 430 nm (for Ag NPs) and at 540 nm (for Au NPs), which indicates the formation of Ag and Au NPs (Fig. S1). The HR-TEM images (Fig. 1) of the Ag (Fig. 1*a*) and Au (Fig. 1*b*) NPs reveal that they are well dispersed without much agglomeration. The Ag and Au NPs are spherical in shape with an average size ranging from 5 to 40 nm (Fig. S2). EDS analysis points out Ag (Fig. S3) as the predominant element, which further substantiates the inferences made from the UV–visible absorption spectra (Fig. S1). ICP-MS analysis reveals that the concentration of Ag and Au is 624 and 548 μg/mg of powder, respectively.

FT-IR spectra (Fig. 2) indicate the formation of IR bands at 631, 1058, 1397, 1623, and 3392 cm^{-1} for the *BOL* extract (Fig. 2*a*), at 632, 1077, 1385, 1627, and 3370 cm^{-1} for the Ag NPs (Fig. 2*b*), and at 3360, 2927, 1621, 1321, 1221, and 1043 for the Au NPs (Fig. 2*c*). The IR bands observed around 1623, 3392, and 1397 cm^{-1} can be assigned to the amide I bond of proteins arising due to carbonyl stretching in proteins, OH stretching vibrations in alcohols and phenolic compounds, and C–N stretching of aromatic amines, respectively. The presence of these bands in the *BOL* extract as well as in both the Ag and Au NPs suggests the involvement of phenolic and carbonyl groups during the synthesis of the Ag and Au NPs. Phenolic compounds, due to their chelating ability, easily form complexes with different metals. Similarly, the carbonyl group of amino acid residues has been shown to strongly bind with

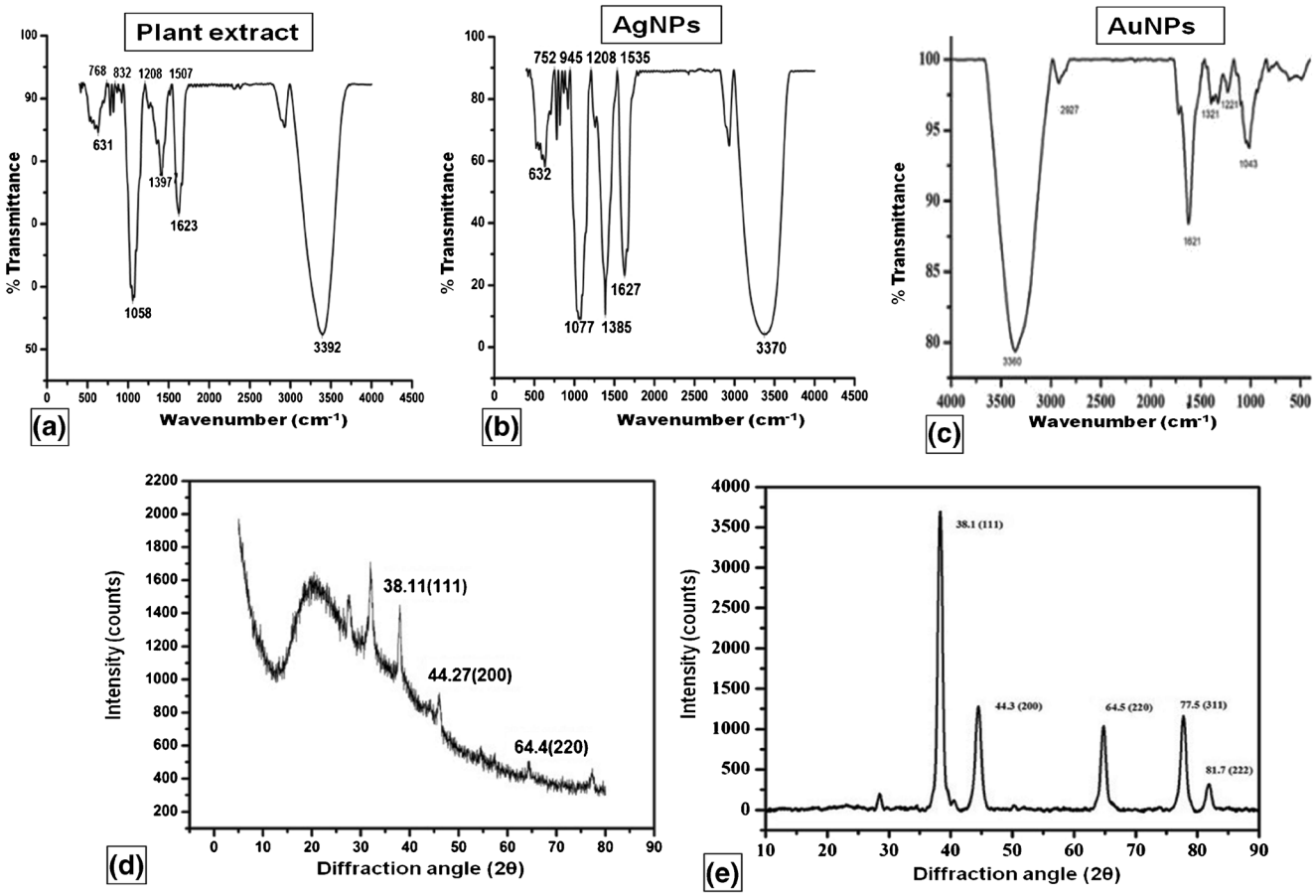

Fig. 2. Nature of functional groups and structure of the *BOL* extract and Ag and Au NPs assessed by *a–c* FT-IR spectra and *d*, *e* XRD patterns. (*a*) FT-IR spectrum of *Brassica oleracea* L. var. *capitata* f. *rubra* extract alone. (*b*) FT-IR spectrum of Ag NPs. (*c*) FT-IR spectrum of Au NPs. (*d*) XRD spectrum of Ag NPs. (*e*) XRD spectrum of Au NPs.

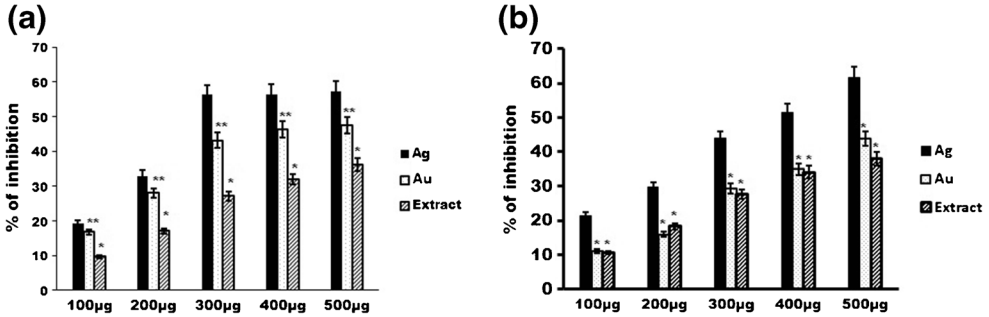

Fig. 3. (*a*) DPPH radical scavenging activity of Ag NPs (100, 200, 300, 400, and 500 μM) and Au NPs (100, 200, 300, 400, and 500 μM). The absorbance values were converted to scavenging effects (percent). (*b*) ABTS radical scavenging activity of Ag NPs (100, 200, 300, 400, and 500 μM) and Au NPs (100, 200, 300, 400, and 500 μM). The absorbance values were converted to scavenging effects (percent). Values are means ± SD of six determinations; **significant compared to Ag NPs at $p < 0.05$; *significant compared to Au NPs at $p < 0.05$.

metal and to act as a capping agent preventing agglomeration of metal NPs (Sharma et al. 2014). Hence, it is clear that the phenolic group present in the *BOL* extract is responsible for reduction of Ag and Au ions while the proteins provide a stabilizing effect which prevented their agglomeration. The XRD patterns of the Ag (Fig. 2*d*) and Au (Fig. 2*e*) NPs reveal the formation of well-defined diffraction peaks, suggesting their crystalline nature. The characteristic diffraction peaks indexed at $2\theta = 38.11°$ (111), 44.27° (200), and 64.4° (220) of Ag matched with JCPDS file no. 04-0783. Similarly, the characteristic diffraction peaks indexed at $2\theta = 38.1°$ (111), 44.3° (200), 64.5° (220), 77.5° (311), and 81.7° (222) of fcc Au matched with JCPDS file no. 04-0783. Based on the diffraction patterns, the Ag and Au NPs can be categorized as face-centered cubic crystals.

Evaluation of antiradical activity of Ag and Au NPs The antiradical property of Ag and Au NPs was evaluated using DPPH· and $ABTS^{\cdot+}$ assays. A comparison of the DPPH· radical scavenging activity of the *BOL* extract with that of the Ag and Au NPs prepared using the extract is presented in Fig. 3*a*. It is evident that all of them exhibited a strong DPPH· radical scavenging property. For a given concentration of 500 μg, the DPPH· radical scavenging ability of the *BOL* extract, Ag NPs, and Au NPs was 36.17, 57.40, and 47.48%, respectively. For the same concentration, the percentage inhibition of $ABTS^{\cdot+}$ for the *BOL* extract, Ag NPs, and Au NPs is 38.04, 61.70, and 43.83%, respectively (Fig. 3*b*). The DPPH assay measures the ability of compounds to act as free radical scavengers or reflects their antioxidant capacity by donating hydrogen ions. It has been reported that Ag and Au NPs prepared by the green synthesis route have the tendency to scavenge free radicals by either donating or accepting electrons based on reaction conditions. The change in the color of the solution from deep purple to stable light yellow depends on the hydrazine molecule upon accepting electrons or hydrogen ions (Sivakumar et al. 2014). Moreover, it is believed that the free radical ability of metal nanoparticles possesses some metal chelation or hydrogen donating activity that could help to prevent free radical formation. In this present study, Ag and Au NPs synthesized using the *BOL* extract exhibited their ability to scavenge DPPH· and $ABTS^{\cdot+}$ radicals. The antioxidant behavior of Ag and Au NPs has made them useful in therapy for many diseases including cancer. They are also being investigated as drug carriers (Ramar et al. 2015).

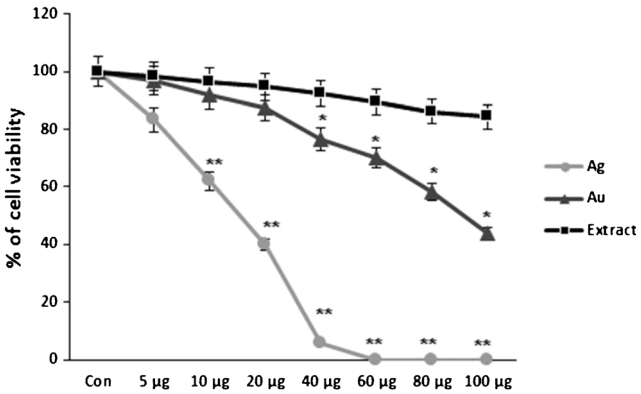

Fig. 4. Ag NPs and Au NPs inhibit cell death in HT-1080 cells. The HT-1080 cells were treated with different concentrations of nanoparticles, and cell proliferation was detected by MTT assay. Values are means ± SD of six determinations; *significant compared to the extract at $p < 0.05$; **significant compared to Ag NPs at $p < 0.05$.

In vitro anticancer studies of Ag and Au NPs using cell culture. Evaluation of cytotoxicity by MTT assay and apoptotic morphology by AO/EtBr staining The in vitro cytotoxicity/apoptosis of the biologically synthesized Au and Ag NPs was analyzed by MTT assay. Figure 4 shows the cytotoxic effects of different concentrations of Ag and Au NPs on HT-1080 cells in terms of percentage of cell viability. The IC_{50} value of the Au and Ag NPs was found to be 93.2 and 18.5%, respectively. Based on these results, ~1/2 IC_{50} dose, viz, 20 μg/ml of Ag NPs and 100 μg/ml of Au NPs, was selected for further biochemical and apoptosis studies. The effect of Ag and Au NPs in inducing toxicity to the

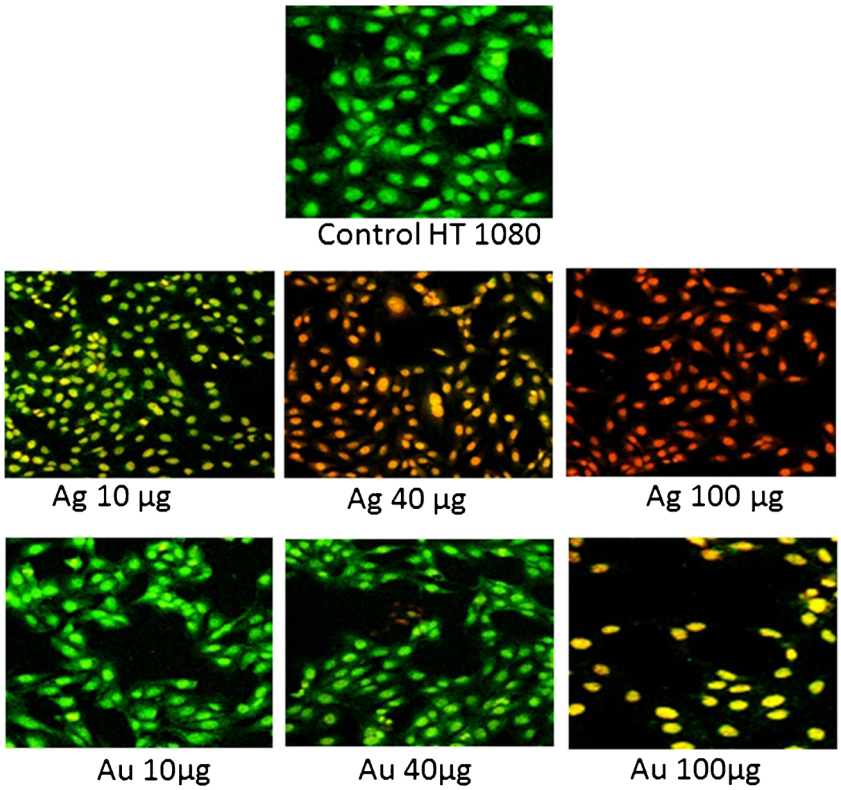

Fig. 5. Cellular morphological changes were observed under a fluorescence microscope using OA/EtBr staining (×20). More apoptotic cells (*red/orange color*) were observed in HT-1080 cells treated with Ag NPs (from 20 µg) and Au NPs (from 80 µg). Con-control

cell is considered to be an early step of apoptosis and DNA condensation (Kulandaivelu and Gothandam 2016). Moreover, nuclei morphological changes were observed in MCF-7 cells after treatment with Ag NPs using *Annona squamosa* leaf extract (Vivek et al. 2012). All these results were consistent with our present study, in which observations

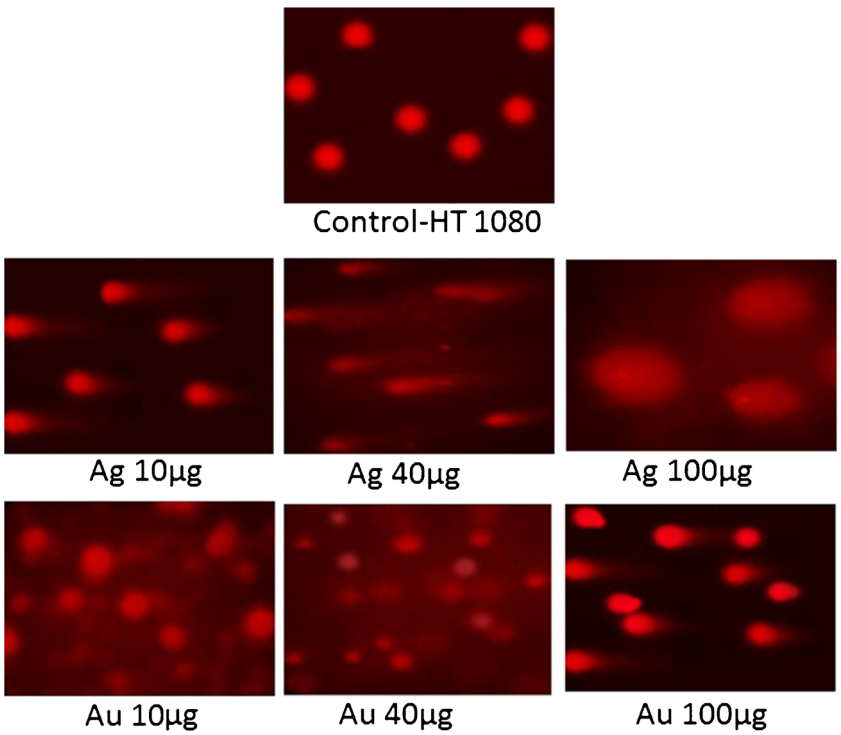

Fig. 6. Ag NPs and Au NPs induced DNA damage attributes in HT-1080 cells. Fluorescence photomicrographs showing an enhanced comet tail in Ag NP- and Au NP-treated HT-1080 cells; *Brassica oleracea* L. var. *capitata* f. *rubra* extract showed no changes in comet formation.

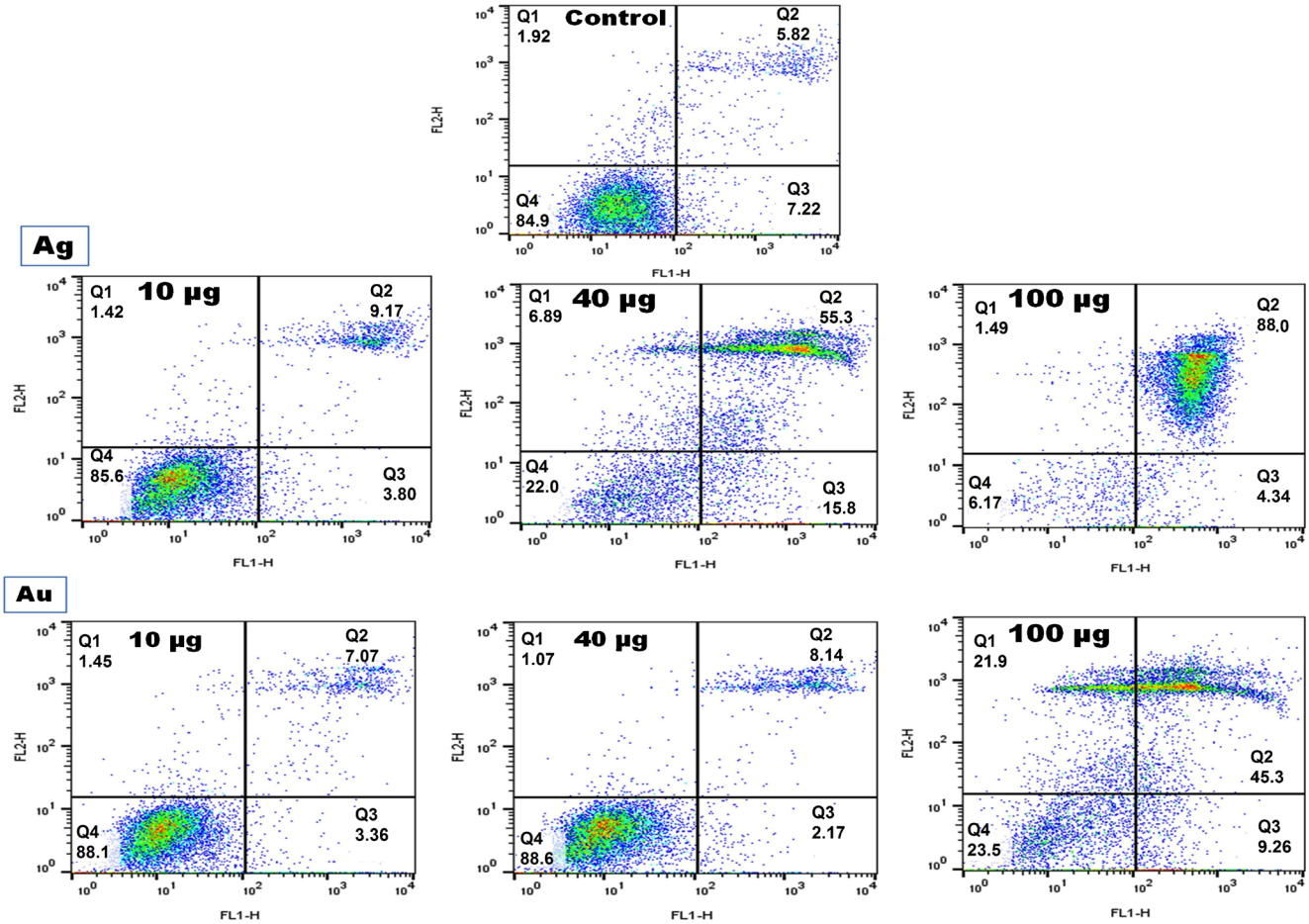

Fig. 7. Apoptosis and necrosis rates induced by Ag NPs and Au NPs in HT-1080 cells.

of apoptosis were noticed with the chromatin condensation and morphological changes in cell shape shown by AO/EtBr staining. The stained cells were characterized as viable (light green), early apoptotic (bright green fluorescence and condensed chromatin), late apoptotic (orange fluorescence), and nonviable (red fluorescence). The untreated cells exhibited much better cell viability without any signs of apoptosis. In contrast, the viability of the cells treated with Ag and Au NPs was found to be dose dependent. For Ag NPs, most of the cells were viable at 5 μg while early apoptosis became visible from 10 to 40 μg. Signs of late apoptosis of cells could be seen beyond 40 μg while complete cell death is evident beyond 80 μg of Ag NPs (Fig. 5). For Au NPs, most of the cells were viable up to 40 μg while early apoptosis became visible from 60 μg. Signs of late apoptosis of cells could be seen beyond 100 μg of Au NPs (Fig. 5). These morphological changes were due to the activation of caspase cascades, which cleaves specific substrates responsible for DNA damage and DNA condensation. It is well known that an extensive DNA insult triggers cell death or apoptosis. A previous report stated that the green synthesis of Ag and Au NPs induced cell death and apoptosis against C2C12 cancer cells, HeLa cells, and HCT-29 cells in a dose-dependent manner (Hu et al. 2010). It is clear from our results that the cytotoxic effect exerted by the Ag and Au NPs was associated with the generation of reactive oxygen species (ROS), which might have contributed to apoptosis and DNA damage in the HT-1080 cancer cells.

Single-cell gel electrophoresis (comet assay) Comet assay was carried out in order to confirm the apoptotic changes induced by the Ag and Au NPs in the HT-1080 cells. Figure 6 illustrates the occurrence of DNA damage in terms of formation of DNA in the tail and variation in tail length, observed at a dose of 10 μg for the Ag NP-treated cells and at a dose of 100 μg for the Au NP-treated cells. In contrast, no such changes were observed for the untreated control cells. An increase in the concentration of Ag NPs leads to a significant increase in the percentage of formation of DNA tail length, which clearly substantiates the occurrence of DNA damage. These findings are in line with previous reports, which show an increase in DNA tail length by comet analysis and DNA fragmentation assay measured by DNA strand break, following induction of Ag and Au NPs in MCF-7, HL-60, and HCT-15 cancer cells. Induction of DNA single-strand break has

often been used to predict oxidative damage of tumor cells induced by NPs (Jeyaraj et al. 2013a). The findings of the present study are in good agreement with the previous work, in which ZnO nanoparticles induced oxidative stress in mitochondria and the nucleus that facilitates apoptosis through DNA fragmentation (Guo et al. 2010). It has also been shown that treatment of Ag and Au NPs caused an increase in the number of tail DNA, tail length, tail moment, and olive tail moment in HeLa cells (Jeyaraj et al. 2013b).

Determination of apoptosis and necrosis Figure 7 shows the representative Annexin V/PI results of the HT-1080 cells treated with varying concentrations of Ag and Au NPs. Cells treated with 10, 40, and 100 μg/ml of Ag NPs exhibited early stages of apoptosis, amounting to 3.80, 15.8, and 4.34%, respectively. However, cells treated with 40 and 100 μg/ml of Ag NPs revealed late apoptosis in the range of 55.3 and 88.0%, respectively. In contrast, for the HT-1080 cells treated with Au NPs, late apoptosis or necrosis is observed beyond 60 μg/ml. For 60 and 100 μg/ml of Au NPs, late apoptosis was found at 43.4 and 45.30%, respectively. These results point out that Ag NPs could induce not only apoptosis as reported but also necrosis in cancer cells, which implies that treatment using Ag NPs could cause inflammatory responses.

Ag and Au NPs induce apoptosis via caspase- and inflammatory-dependent pathways detected by qRT-PCR and western blot Cell death or apoptosis and inflammatory pathways are induced by Ag and Au NPs through excessive production of ROS made by oxidative stress. The activation of cas-3 and cas-7 plays an important role in several apoptotic mechanisms. Similarly, the activation of TNF-α and NF-κB is responsible for inflammatory pathways. In our study, the mRNA and protein expression of cas-3, cas-7, TNF-α, TGF-β, and NF-κB were detected by RT-PCR and western blot analysis. A list of primers used in this study is given in Table 2. The mRNA expression of cas-3, cas-7, TNF-α, and NF-κB was significantly upregulated for the HT-1080 cells treated with 40 μg of Ag NPs and 100 μg of Au NPs when compared to the control cells (Fig. 8*A*). These inferences reveal that the major mode of cell death occurred through activation of apoptosis (cas-3 and cas-7) and inflammatory (TNF-α and NF-κB) pathways induced by Ag and Au NPs. The activation of TNF-α and NF-κB initiated the destruction of mitochondria, which provoked the release of apoptogenic factors, resulting in cell death (Sivakumar and Anuradha 2011). Effector caspases execute major apoptotic changes in cells, resulting in DNA fragmentation and degradation of nuclear and cytoskeletal proteins, which successfully lead to apoptosis. The findings of the present study reveal that Ag and Au NPs derived using the *BOL* extract possess potent anticancer activity, which is evidenced by their ability to induce apoptosis and inflammation in HT-1080 cancer cells, through the activation of cas-3, cas-7, TNF-α, and NF-κB.

The generation of ROS could influence the expression/activation of NF-κB while NF-κB can induce the synthesis of TNF-α and IL-6. Figure 8*B* depicts the western blot analysis of NF-κB, which shows that p65 in nuclear fractions were significantly upregulated in the HT-1080 cancer cells treated with Ag and Au NPs, when compared to the untreated cells. This inference confirms the increased translocation of NF-κB into the nucleus from the cytoplasm for the cells treated with Ag and Au NPs. Under normal conditions, NF-κB is sequestered and exists in an inactive form in the cytoplasm, so it cannot translocate into the nucleus. We suggest that inflammatory factors such as Ag and Au NPs, which can initiate NF-κB activation in the cytoplasm, are further translocated to the nucleus, which in turn initiate inflammatory reactions (Sivakumar and Anuradha 2011). Hence, our present study has proved that Ag and Au NPs damage DNA and activate inflammatory and apoptotic pathways, following their ability to penetrate into cells through ion channels, resulting in damage of the cell membrane.

Mode of interaction of Ag and Au NPs with HT-1080 cell membranes The effect of intercellular uptake of Ag and Au NPs in HT-1080 cells is clearly depicted in Fig. 9. It is evident that the Ag NPs (20 μg) and Au NPs (80 μg) penetrated the cytoplasm and nucleus, resulting in apoptotic morphological changes through subsequent loss of the cell membrane and

Table 2. Primer sequences

Gene	Primer sequences (5′–3′)	Amplicon length (bp)	Annealing temperature (°C)
cas-3	F-ATGGAAGCGAATCAATGGAC	596	60.1
	R-ACAAAGCGACTGGATGAACC		
cas-7	F-TATTGAAGAGCAGGGGGTTG	539	60.01
	R-GGCAAGCCTGAATGAAGAAG		
TNF-α	F-TGCTTGTTCCTCAGCCTCTT	564	60.47
	R-ATAGTCGGGCCGATTGATCT		
NF-κB	F-TGGAAGCACGAATGACAGAG	544	60.00
	R-CGAAGCTGGACAAACACAGA		

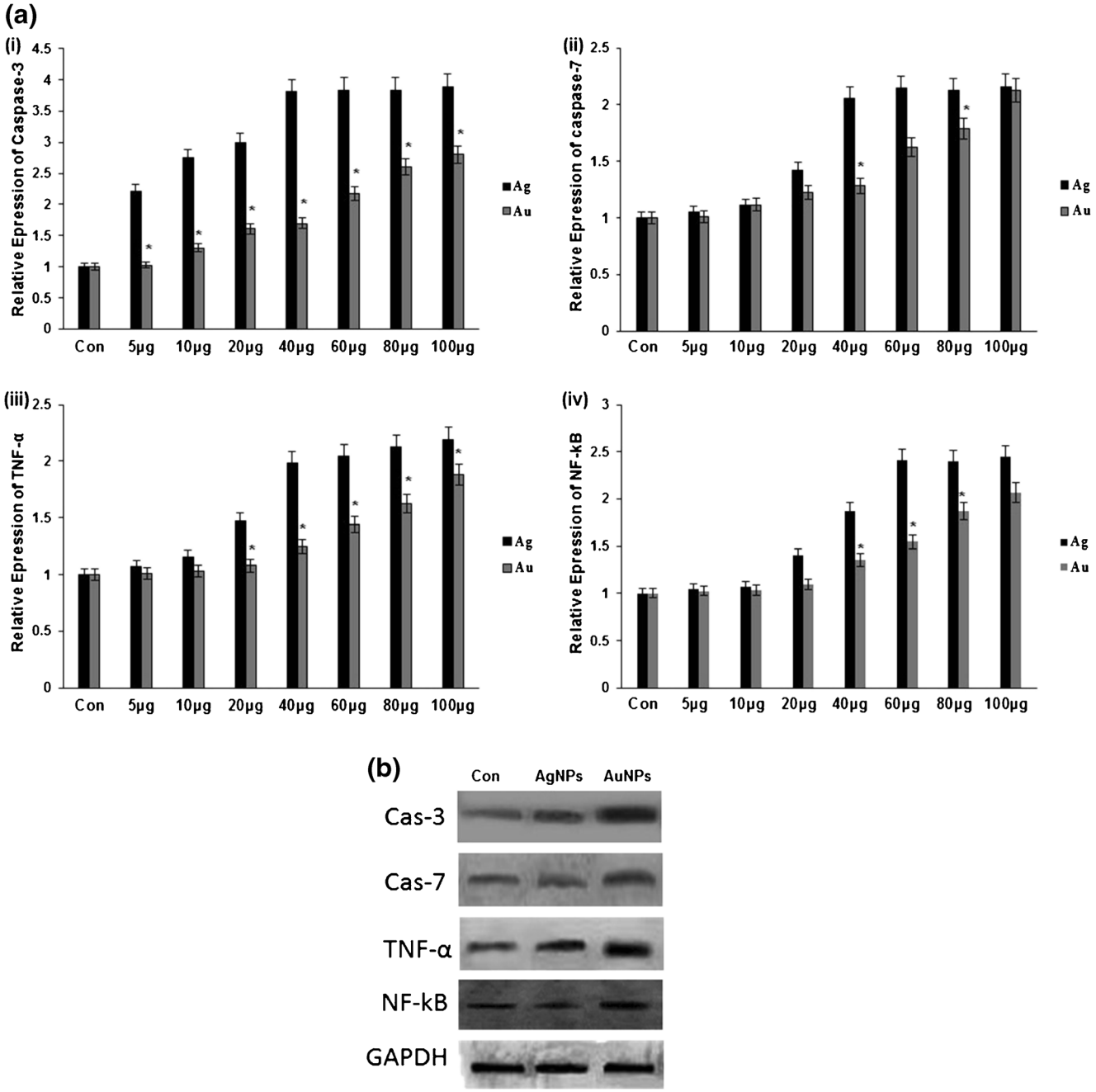

Fig. 8. (*a*) Bar diagram representing the RT-PCR analysis of caspase-3 *(i)*, caspase-7 *(ii)*, TNF-α *(iii)*, and NF-κB *(iv)*. The results depicted are normalized to the levels of GAPDH and expressed relative to the control. (*b*) Western blot analysis of HT-1080 cells with Ag NPs (20 μg) and Au NPs (80 μg), showing decreased in caspase-3, caspase-7, TNF-α, and NF-κB (nuclear fractions) when compared to the untreated cells. Values are means ± SD of six determinations; *significant compared to Ag NPs at $p < 0.05$.

mitochondrial membrane. In addition, changes in morphological features have also confirmed the reduction of microvilli density, ruptured plasma membrane, and bleb development. In contrast, the control cells are much healthier than those treated with Ag and Au NPs. In general, NPs have the ability to penetrate the cell membrane and strongly interact with cells and intracellular macromolecules like proteins and DNA, leading to cell death (Jeyaraj et al. 2013b). NPs have the potential to easily penetrate the nuclear membrane, causing cytotoxicity and other cellular responses, which include (i) plasma membrane damage that might cause instability associated with ion transport and signal transduction; (ii) interaction with mitochondria, which may alter antioxidant defenses and ROS production leading to membrane injury; (iii) interaction with DNA, which might cause DNA damage, alteration in cell cycle division leading to cell cycle arrest and protein

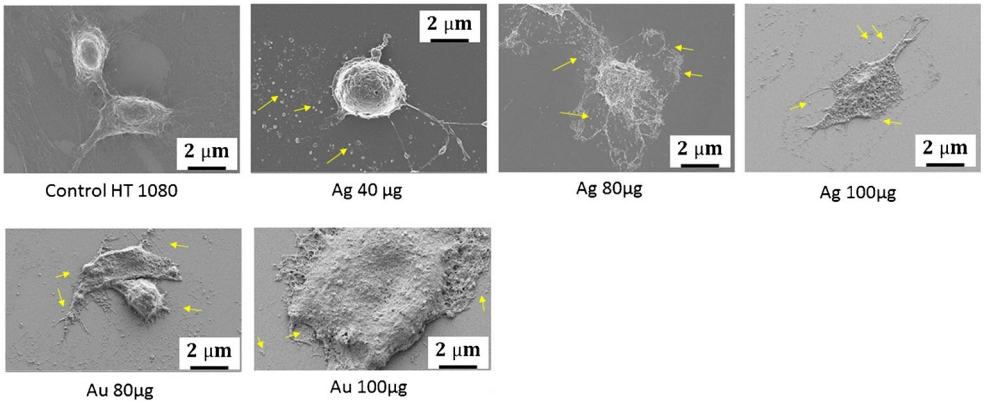

Fig. 9 . Nanoparticle detection inside cells of a HT-1080. The white dots (*yellow arrows*) are nanoparticles, and they are ruptured in the cell membrane and enter into the cytoplasm; the nucleus is well resolved in the image despite being located inside the cell.

denaturation or degradation causing loss of enzyme activity; and (iv) interaction with proteins, lipids, and other biomolecules, which may lead to different types of "corona" and biological effects including inflammation. The findings of the present study further substantiate that Ag and Au NPs internalize inside the cells and cause cell death. The results of the present study are in agreement with an earlier report, which shows the effect of Ag NPs on MCF-7 cells and Au NPs on SK-BR-3 cells, causing a variation in cell shape, like coiling and cell shrinkage, when compared to the respective control cells (Foldbjerg et al. 2009).

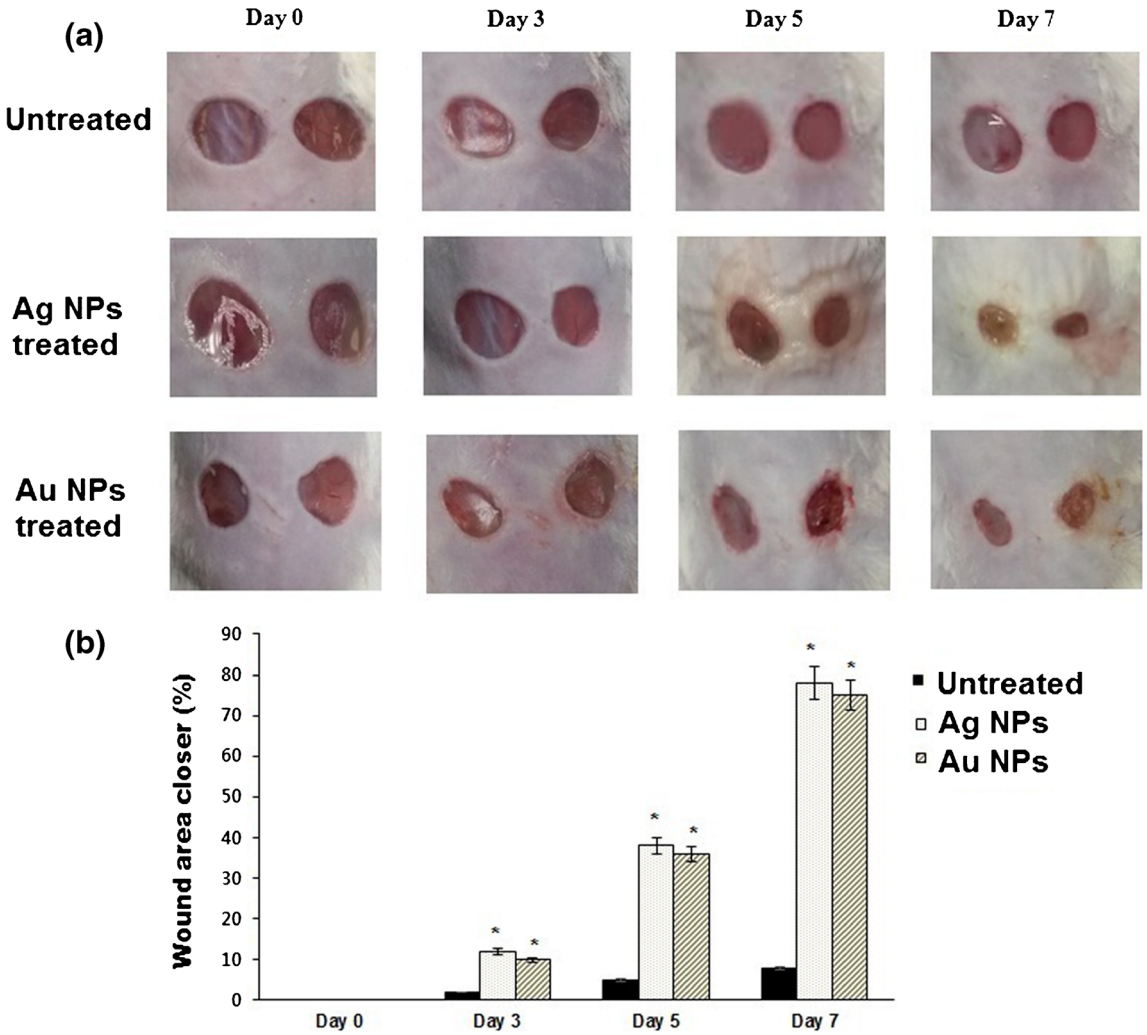

Fig. 10. (*a*) Ag NPs and Au NPs accelerate skin wound healing. Time taken for skin wounds to heal in mice treated with Ag NPs and Au NPs. Values are expressed as percentage of wound area closure. (*b*) Values are means ± SD of six determinations; *significant compared to control at $p < 0.05$.

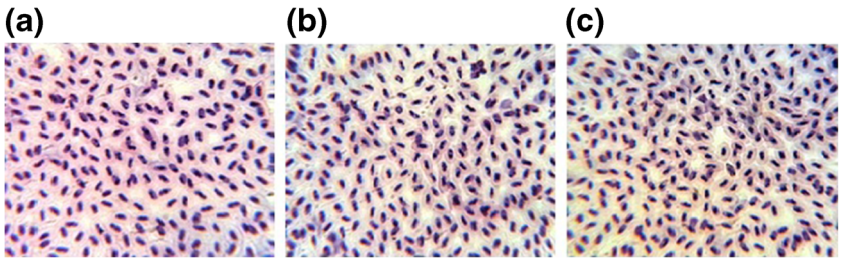

Fig. 11. Photomicrographs of erythrocytes with a normal nucleus in the peripheral blood cells of (a) control (b) Ag NP and (c) Au NP-treated ICR mice during wound healing.

In vivo toxicity and wound healing Skin wound healing is considered to be a complex biological process that warrants cellular interaction between varieties of cells including immune cells. The effect of Ag and Au NPs on wound healing is depicted in Fig. 10. It is evident that wound closure was observed in all treatment groups within 7 d. In fact, treatment with both the Ag and Au NPs exhibited excellent healing effect even from the 3rd day after surgery. The observed acceleration in wound healing and the decrease in scar size are believed to occur due to an increase in immunity and improved antibacterial effect imparted by the Ag and Au NPs. Treatment with the Ag NPs led to increase in inflammatory factors such as TNF-α and TGF-β. The findings of this study demonstrate that both the Ag and Au NPs prepared using the *BOL* extract have potential application in wound dressing. It has been reported that treatment with Ag NPs during wound healing exhibits no toxic effect on blood parameters such as AST, ALT, red blood cells, and white blood cells (Percival et al. 2005). In order to confirm the toxic effect of Ag and Au NPs during the period of wound healing, the activity of AST and ALT in the plasma of experimental animals was monitored. No significant changes in AST and ALT could be found among the tested groups (Table 1). Hence, it is clear that both the Ag and Au NPs of the present study did not cause any toxic effect during wound healing.

MN and NA tests using PAS staining In addition to oxidative stress, a sign of genotoxic activity was also observed in various parts of the Ag NP- and Au NP-exposed animals. During the wound healing process, micronuclei (MN) and nuclear abnormalities (NA) such as blebbed nuclei, lobed nuclei, and notched nuclei were not observed in the peripheral blood erythrocytes of the Ag NP- and Au NP-treated ICR mice (Fig. 11).

Conclusion

In conclusion, (i) the *BOL* extract could be successfully used to synthesize Ag and Au NPs, thus making it as a feasible green synthesis route. (ii) Ag and Au NPs displayed free radical scavenging activity. (iii) Intracellular uptake of NPs into HT-1080 cells was confirmed by electron microscopy study. (iv) Ag and Au NPs induced protein and gene expression of TNF-α, NF-κB, cas-3, and cas-7 involved in apoptosis. (v) Induction of apoptosis and DNA damage was further confirmed by MTT assay, AO/EtBr staining, and comet assay. (vi) Both Ag and Au NPs could effectively transfer into cells and induce free radical scavenging activity, and Ag NPs displayed better antioxidant activity than Au NPs. (vii) Ag NPs induced apoptosis, gene expression, protein activation, and cell death significantly at lower concentrations around 40 μg whereas for Au NPs, such occurrences are feasible up to 80 μg. All these results clearly point out that the choice of Ag NPs for cancer treatment is better than that of Au NPs. (viii) Ag NPs accelerate wound healing, while no clear toxic effects in biochemistry and hematological parameters were verified in all the treated groups. From our findings, we conclude that a lower concentration of Ag NPs derived from the *BOL* extract activates apoptotic and inflammatory pathways, which induces death of cancer cells. Moreover, this work demonstrated an interesting formulation to treatment of biogenic Ag NPs that improved wound healing and did not exhibit clearly in vivo toxicity than Au NPs.

Acknowledgements The TEM and SEM samples were analyzed using the JEM-2010 (JEOL) installed at the Center for University-Wide Research Facilities (CURF) at Chonbuk National University. We thank Mrs. Eun-Jin Choi at the CURF at Chonbuk National University.

Compliance with ethical standards All procedures relating to the animals and their care conformed to the international guideline "Principles of Laboratory Animals Care" (NIH Publication No. 85-23, revised 1985).

References

Ahmed MF, Rao A (2014) Simultaneous determination of phenolic compounds in *Brassica oleracea L. var capitata*. by high-performance liquid chromatography. Int J Pharm Pharm Sci 6:534

Brand-Williams W, Cuvelier ME, Berset CLWT (1995) Use of a free radical method to evaluate antioxidant activity. LWT-Food Sci Tech 28:25

Foldbjerg R, Olesen P, Hougaard M, Dang DA, Hoffmann HJ, Autrup H (2009) PVP-coated silver nanoparticles and silver ions induce reactive oxygen species, apoptosis and necrosis in THP-1 monocytes. Toxicol Lett 190:156

Guo H, Qian H, Idris NM, Zhang Y (2010) Singlet oxygen-induced apoptosis of cancer cells using upconversion fluorescent nanoparticles as a carrier of photosensitizer. Nanomed Nanotech 6:486

Hu W, Lee SK, Jung MJ, Heo SI, Hur JH, Wang MH (2010) Induction of cell cycle arrest and apoptosis by the ethyl acetate fraction of Kalopanax pictus leaves in human colon cancer cells. Bioresour Technol 101:9366

Jeyaraj M, Rajesh M, Arun R, MubarakAli D, Sathishkumar G, Sivanandhan G, Dev GK, Manickavasagam M, Premkumar K, Thajuddin N, Ganapathi A (2013a) An investigation on the cytotoxicity and caspase-mediated apoptotic effect of biologically synthesized silver nanoparticles using Podophyllum hexandrum on human cervical carcinoma cells. Colloids Surf B Biointerfaces 102:708

Jeyaraj M, Sathishkumar G, Sivanandhan G, MubarakAli D, Rajesh M, Arun R, Kapildev G, Manickavasagam M, Thajuddin N, Premkumar K, Ganapathi A (2013b) Biogenic silver nanoparticles for cancer treatment: an experimental report. Colloids Surf B Biointerfaces 106:86

Kulandaivelu B, Gothandam KM (2016) Cytotoxic effect on cancerous cell lines by biologically synthesized silver nanoparticles. Braz Arch Boil technol 59:1

Kumar CG, Mamidyala SK (2011) Extracellular synthesis of silver nanoparticles using culture supernatant of Pseudomonas aeruginosa. Colloids Surf B 84:462

Lafon-Hughes L, Di Tomaso MV, Mendez-Acuna L, Martınez-Lopez W (2008) Chromatin-remodelling mechanisms in cancer. Mutat Res 658:191

Lakshmi S, Dhanya GS, Joy B, Padmaja G, Remani P (2008) Inhibitory effect of an extract of Curcuma zedoariae on human cervical carcinoma cells. Med Chem Res 17:335

Liu H, Xu Y, Wen S, Zhu J, Zheng L, Shen M, Zhao J, Zhang G, Shi X (2013) Facile hydrothermal synthesis of low generation dendrimer-stabilized gold nanoparticles for in vivo computed tomography imaging applications. Polym Chem 4:1788

Livak KJ, Schmittgen TD (2001) Analysis of relative gene expression data using real-time quantitative PCR and the $2^{-\Delta\Delta CT}$ method. Methods 25:402

Nasongkla N, Bey E, Ren J, Ai H, Khemtong G, Guthi JS, Chin SF, Sherry AD, Boothman DA, Gao J (2006) Multifunctional polymeric micelles as cancer-targeted, MRI-ultrasensitive drug delivery systems. Nano Lett 6:2427

Pardee AB, Stein GS (2011) The biology and treatment of cancer: understanding cancer. Wiley, Hoboken

Percival SL, Bowler PG, Russell D (2005) Bacterial resistance to silver in wound care. J Hosp Infect 60:1

Pradeep T (2009) Noble metal nanoparticles for water purification: a critical review. Thin Solid Films 517:6441

Ramar M, Manikandan B, Marimuthu PN, Raman T, Mahalingam A, Subramanian P, Karthick S, Munusamy A (2015) Synthesis of silver nanoparticles using Solanum trilobatum fruits extract and its antibacterial, cytotoxic activity against human breast cancer cell line MCF 7. Spectro chimica Acta A 140:223

Saha K, Agasti SS, Kim C, Li X, Rotello VM (2012) Gold nanoparticles in chemical and biological sensing. Chem Rev 112:2739

Salunke GR, Ghosh S, Kumar RS, Khade S, Vashisth P, Kale T, Chopade S, Pruthi V, Kundu G, Bellare JR, Chopade BA (2014) Rapid efficient synthesis and characterization of silver, gold, and bimetallic nanoparticles from the medicinal plant Plumbago zeylanica and their application in biofilm control. Int J Nanomedicine 9:2635

Sharma G, Sharma AR, Kurian M, Bhavesh R, Nam JS, Lee SS (2014) Green synthesis of silver nanoparticle using Myristica fragrans (nutmeg) seed extract and its biological activity. Dig J Nanomater Biostruct 9:325

Singh NP, McCoy MT, Tice RR, Schneider EL (1988) A simple technique for quantitation of low levels of DNA damage in individual cells. Exp Cell Res 175:184

Singh J, Upadhyay AK, Bahadur A, Singh B, Singh KP, Rai M (2006) Antioxidant phytochemicals in cabbage (Brassica oleracea L. var. capitata). Sci Hortic-Amsterdam 108:233

Singh S, Jain DVS, Singla ML (2013) Sol–gel based composite of gold nanoparticles as matix for tyrosinase for amperometric catechol biosensor. Sensor Actuat B-Chem 182:161

Sivakumar AS, Anuradha CV (2011) Effect of galangin supplementation on oxidative damage and inflammatory changes in fructose-fed rat liver. Chem Biol Interact 193:141

Sivakumar AS, Ochirbat C, Cho SH, Yang J, Hwang I (2014) Antiapoptotic effect of a novel synthetic peptide from bovine muscle and MPG peptide on H2O2-induced C2C12 cells. In vitro cell dev biol anim 50:630

Vivek R, Thangam R, Muthuchelian K, Gunasekaran P, Kaveri K, Kannan S (2012) Green biosynthesis of silver nanoparticles from Annona squamosa leaf extract and its in vitro cytotoxic effect on MCF-7 cells. Process Biochem 47:2405

Woolfenden BS, Wilson RL (1982) Radical cations as reference chromogens in studies of one-electron transfer reactions: pulse radiolysis studies of 2, 2-azinobis-(3-ethylbenzthiazoline-6-sulfonate). J Chem Soc Perkin Trans:805–812